Available online at www.sciencedirect.com
SCIENCE DIRECT®
Polymer 45 (2004) 1923–1932
polymer
www.elsevier.com/locate/polymer

P(VDF-TrFE)-layered silicate nanocomposites. Part 1. X-ray scattering and thermal analysis studies

Peggy Cebe[a,*], James Runt[b]

[a]Department of Physics and Astronomy, Tufts University, STC-208, 4 Colby Street, Medford, MA 02155, USA
[b]Department of Materials Science and Engineering, Pennsylvania State University, University Park, PA 16802, USA

Received 20 November 2003; accepted 12 January 2004

Abstract

X-ray scattering and thermal analyses were used to investigate the effects of organically modified layered silicates (OMS) on the paraelectric and ferroelectric phase transitions in poly(vinylidene fluoride-co-trifluoroethylene) [P(VDF-TrFE)]/OMS nanocomposites. Nanocomposites comprising a 75/25 P(VDF-TrFE) random co-polymer with either Nanomer I.30TC or Lucentite STN OMS were prepared with compositions ranging from 2 to 25 wt% OMS. Wide-angle X-ray scattering (WAXS) studies show that the silicate gallery spacing increases modestly in the nanocomposites compared to the neat OMS powder, indicating a level of co-polymer intercalation. Thermogravimetric analysis indicates that thermal stability is improved in nanocomposites with higher OMS contents: they have substantial increase in weight remaining, both at 500 °C and at 1000 °C, compared to that predicted from the behavior of the neat co-polymer and OMS. Differential scanning calorimetry (DSC) and WAXS results show that thermal transitions in the nanocomposites depend on OMS content. Nanocomposites with 2% OMS exhibited a crystal nucleating effect, which results in significant increase in the amount of ferroelectric crystals formed during cooling. For greater OMS additions (10–25%), the amounts of para- and ferroelectric crystals are reduced. The larger OMS additions depress the melt-to-paraelectric transition temperature, while an increase in the paraelectric-to-ferroelectric transition temperature is observed for all compositions. Upon reheating, the ferroelectric phase transition shows significant hysteresis. We conclude that the addition of either Lucentite or Nanomer OMS to 75/25 P(VDF-TrFE) causes an *increase* in the temperature stability range for the ferroelectric phase.

Keywords: Ferroelectric; Organically modified silicates; P(VDF-TrFE) co-polymer

1. Introduction

Poly(vinylidene fluoride) and its random co-polymers with trifluoroethylene [P(VDF-TrFE)] exhibit spontaneous electrical polarization, or, ferroelectricity, upon cooling from the melt [1–3]. Because of the high electro-negativity of the fluorine atoms, the monomer units of PVDF contain an intrinsic dipole moment, but in the melt, the chains are randomly oriented so the melt itself is non-polar. Upon cooling, PVDF crystallizes in a variety of crystallographic forms [4] but the all-trans beta phase (also called Phase I) is of interest in the present work. In the beta phase the monomer dipole moments orient and crystallize into a polar, non-centrosymmetric, crystal unit cell.

The addition of either tetra- or tri-fluoroethylene units into the polymer chain introduces head-to-head defects [5], and causes the co-polymer to crystallize readily into the electrically active beta phase. During cooling from the non-polar melt, the paraelectric crystal phase forms first, in which the molecules are described [6] as partly disordered through introduction of *gauche* ± bonds [6]. Further cooling results in transformation to the ferroelectric crystal phase with structure similar to the PVDF beta phase.

P(VDF-TrFE) random copolymers with VDF content between ~50 and 80 mol% are strongly piezo- and pyroelectric [7] and are used in a variety of applications, including electromechanical and data storage devices [4,8]. These copolymers are semi-crystalline and the ferroelectric to paraelectric crystalline phase transition temperature (as well as the corresponding functional properties) are sensitive to copolymer concentration. It has been discovered quite recently that the introduction of defects in P(VDF-TrFE),

* Corresponding author. Tel.: +1-6176273365; fax: +1-6176273744.
E-mail address: peggy.cebe@tufts.edu (P. Cebe).

0032-3861/$ - see front matter © 2004 Elsevier Ltd. All rights reserved.
doi:10.1016/j.polymer.2004.01.014

either by exposure to high energy electron irradiation [9], chemical crosslinking [10], or by incorporating a modest amount of termonomer [11,12] into the chain structure leads to marked changes in electromechanical properties, including dramatic improvements in electrostrictive strain.

Unlike many random copolymers, relatively high degrees of crystallinity can be achieved in P(VDF-TrFE) since the H and F atoms are of similar size, and VDF and TrFE (stereo-irregular) behave isomorphically. Unit cell type, crystalline chain conformation, and other characteristics of the β phase of the PVDF homopolymer and P(VDF-TrFE) are the same: the difference is that the P(VDF-TrFE) unit cell is expanded by the presence of TrFE [13]. The copolymers are capable of crystallizing to quite high degrees (up to 90% when well annealed [14]), with lamellar thicknesses approaching that of the extended chain form, i.e. up to ~100–130 nm [15]. Such large thicknesses can be achieved in these and similar polymers due to activation of a sliding diffusion mechanism upon annealing in the paraelectric hexagonal phase [14].

In the past several years there has been intense interest in polymer-based nanocomposites. The fundamental goal is usually to significantly improve a target property or suite of properties, but at much lower 'filler' content than would be required for additives of traditional size. Considerable success has been achieved by dispersing organically modified layered silicates (OMS) in polymers, particularly for mechanical reinforcement (as a result of their high aspect ratio), but also for improvement in barrier properties and flame retardency [16–18]. For example, we recently used this approach to significantly reduce the gas permeability of biomedical polyurethane elastomers, without loss of ductility [19,20]. Such enhancements are beyond what can be generally achieved through chemical modification of polyurethanes.

In the present paper, we extend our research on OMS nanocomposites to those with a prototypical ferroelectric co-polymer, focusing on the influence of the OMS on the crystallization behavior. Using real-time methods, we investigate the transitions from the melt to the paraelectric state, and then to the ferroelectric state. Calorimetric and scattering data confirm that the addition of OMS reduces the degree of crystallinity, but increases the temperature range for stability of the ferroelectric crystals.

2. Experimental section

2.1. Sample preparation

The P(VDF-TrFE) random co-polymer used in the present study was kindly provided by Dr Mitch Thompson of Measurement Specialties, Inc. in pellet form. The polymer is an Elf Atochem Kynar-based copolymer of vinylidene fluoride and trifluoroethylene in the mol% ratio 75/25. Two OMS were used to prepare composites. The first is Lucentite STN, obtained from Zen-Noh Unico, America. This material was prepared by the supplier by ion-exchanging the Na ions in a synthetic smectite clay (Lucentite SWN, with a cation exchange capacity of approximately 0.65 meq/g) for tri octyl methyl ammonium cations. The second OMS is Nanomer I.30TC obtained from Nanocor, Inc., prepared by the supplier, by ion-exchanging Na^+ MMT with octadecylammonium. The average aspect ratio of Nanomer I.30TC has been reported to be 200–500 [21]. Both OMS materials were obtained as fine powders.

The co-polymer and the OMS materials were first separately dissolved in dimethylacetamide (DMAc) at room temperature with stirring for about 1–2 days. Initial solution concentrations were 0.140 g cm^{-3} (co-polymer/DMAc), and 0.0268 g cm^{-3} (OMS/DMAc). Both the copolymer and the Lucentite OMS formed transparent clear solutions in DMAc, while the Nanomer OMS formed somewhat hazy, translucent mixtures. Next the OMS solution was added to the copolymer solution to achieve the desired weight ratio of OMS to copolymer. The composite compositions reported here are 2, 10, 18 and 25% OMS *by weight*. The mixtures were stirred at room temperature for times ranging from 3 to 10 days. Very strong molecular interaction between the polymer and the OMS is inferred from the color change observed when the OMS was mixed into the polymer solution. Within one day of mixing, Lucentite-co-polymer mixtures became deep red to orange colored, depending upon composition while the Nanomer-co-polymer solutions became deep to pale tan colored upon mixing.

These solutions were poured into uncovered glass Petri dishes, and gently heated at about 40–70 °C for one day, to assist in removal of DMAc. A thin, tough film resulted, that could be easily lifted from the dish. Further drying of the film took place in a vacuum oven at room temperature for 1–2 weeks. The Lucentite composite as-cast films are orange colored, and transparent in all compositions. Nanomer composite as-cast films are tan colored and semi-opaque.

All TGA, DSC, FTIR and X-ray scattering measurements were performed on P(VDF-TrFE)/OMS nanocomposites films cast from solution as described above. In the case of the pure OMS, TGA, FTIR and real-time X-ray scattering measurements were performed on OMS films cast from solution as described above. In one case only was the OMS powder used as received, and that was for static WAXS studies where the gallery spacing of the neat OMS powder was sought.

2.2. Analysis methods

Thermogravimetric analysis of weight loss during heating was performed using a TA Instruments TGA 2050, with nitrogen gas flow rate of 90 cm min^{-3}. The temperature ranged from room temperature to 1000 °C at a

heating rate of 10 °C min^{-1}. Sample mass ranged from 10 to 30 mg.

Infrared studies were performed using a Bruker Equinox 55 FTIR equipped with an attenuated total reflectance (ATR) cell. The resolution was 4 cm^{-1} and 256 scans were co-added to improve the signal to noise. The 75/25 co-polymer and nanocomposite films were studied using the ATR method. The OMS specimen was prepared by spreading a few drops of OMS solution in DMAc onto KBr disks and the FTIR spectrum acquired in transmission. There was no signature of residual DMAc in any of the FTIR scans.

Calorimetric analysis was performed on as-cast films using a TA Instruments 2920 temperature modulated differential scanning calorimeter (TM-DSC). Heating and cooling rates were 5 °C min^{-1} in standard DSC mode. The instrument temperature and heat flow were calibrated using an Indium reference, and the heat capacity was calibrated using a sapphire standard. Sample masses ranged from 3 to 9 mg, and the sample and reference pan weights were matched within 0.05 mg. Nitrogen purge gas flow was 30 ml min^{-1}. The thermal sequence for DSC and X-ray studies was identical: samples were heated from 30 to 170 °C, held isothermally for 2 min, cooled to 50 °C, held isothermally for 2 min, the reheated to 170 °C. In our DSC scans, exotherms are presented with upward departure from the baseline.

Simultaneous, real-time wide and small angle X-ray scattering (WAXS and SAXS) studies were performed at beam line X27C of the National Synchrotron Light Source at Brookhaven National Laboratory. Intensity data were collected during cooling and reheating with films encapsulated in Kapton™ tape and held in a Mettler FP80 hot stage. Monochromatic X-radiation with a wavelength of $\lambda = 0.1366$ nm was used. The data were collected in transmission mode using two one-dimensional position sensitive wire detectors. The scattering vectors, q ($q = 4\pi \sin\theta/\lambda$, for θ the half-scattering angle) were calibrated using sodelite and silicon reference powders for WAXS, and silver behenate for SAXS. Scans were collected for 30 or 60 s over an angular range from $2\theta = 10 - 30°$. Intensity data were corrected to account for detector linearity, background scattering, sample absorption, and changes in incident beam intensity.

Due to the detector geometry, the range of angles from $2\theta = 1 - 7°$ was not accessible at NSLS. Therefore, room temperature WAXS studies were performed using a conventional sealed tube X-ray source having $\lambda = 0.154 \times$ nm. A Phillips PW1830 X-ray generator and optically encoded diffractometer were used to investigate the range of scattering angles at which the OMS typically shows its gallery spacing, i.e. from $2\theta = 2 - 7°$. Films were examined in $\theta/2\theta$ reflection mode, using a step scan interval of 0.01° with 2.4 s/step; d-spacings, obtained from Bragg's Law ($n\lambda = 2d \sin\theta$), were calibrated using sodelite and silicon.

3. Results and discussion

3.1. Thermal analysis

Fig. 1(a) and (b) shows relative weight loss (solid lines), and its derivative (dashed lines), vs. temperature on selected samples. The left vertical axis is scaled from 0 to 100% for each sample shown. The right vertical axis reflects the derivative signals and these are positioned relative to the zero line but are arbitrarily scaled.

Fig. 1 shows that the weight loss in the OMS powder (curve 1, in Fig. 1(a) (Lucentite OMS), and Fig. 1(b) (Nanomer OMS)) begins at lower temperature than the co-polymer (curve 2, Fig. 1(a)) due to loss of the OMS surfactant. Assuming that the surfactant is removed by the time the temperature reaches 550 °C, its amount can be estimated from the weight loss. Table 1 reports the weight lost from 50 to 550 °C, with Lucentite and Nanomer OMS losing, respectively, 29.9 and 33.7% over this temperature range. This result matches well the published range of surfactant contents for these materials [21].

This translates into lower initiation of weight loss in the nanocomposites. However, the overall thermal stability of the composites at very high temperature is significantly

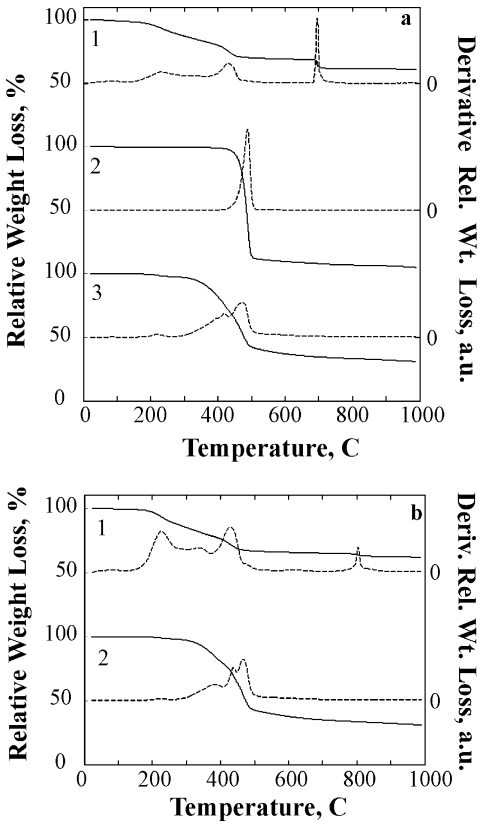

Fig. 1. Relative weight loss (solid lines) and its derivative (dashed lines) vs. temperature during heating at 10 °C min^{-1}. (a) Lucentite OMS (curve 1); 75/25 P(VDF-TrFE) co-polymer (curve 2); 75/25 P(VDF-TrFE) + 18% Lucentite OMS nanocomposite (curve 3). (b) Nanomer OMS (curve 1); 75/25 P(VDF-TrFE) + 18% Nanomer OMS nanocomposite (curve 2).

Table 1
Thermogravimetric analysis—relative weight loss at 550 °C and residue at 1000 °C for P(VDF-TrFE)/OMS nanocomposites, expected and observed values

Sample	OMS (%)	% Wt loss 50–550 °C		% Residue at 1000 °C	
		Expected	Observed	Expected	Observed
75/25[a]	0	89	89	5.2	5.2
N	10	84.3	69.2	12.2	4.2
N	18	79.0	60.0	15.5	31.8
N	25	75.1	60.4	19.4	22.6
N	100	33.7	33.7	62.1	62.1
L	10	83.2	71.9	10.8	6.8
L	18	78.5	61.3	15.2	27.3
L	25	74.5	60.2	19.3	32.3
L	100	29.9	29.9	62.7	62.7

[a] 75/25 refers to copolymer; N refers to Nanomer OMS; L refers to Lucentite OMS.

improved by OMS addition. Table 1 compares the TGA results of both types of composites. In the nanocomposites, the observed weight lost by 550 °C is less than that expected by apportioning the weight loss between polymer and OMS according to the TGA results on the co-polymer and OMS controls. In addition, for compositions of 18 and 25% OMS, the observed residue at 1000 °C is greater than the expected value. Only in the lower composition 10% OMS is the residue at 1000 °C less than anticipated.

Fig. 2 shows the first cooling and second heating DSC scans for co-polymer and nanocomposite films. Fig. 2(a) compares the co-polymer (solid line), and the nanocomposites with 2% Lucentite OMS (dotted line) and 2% Nanomer OMS (dashed line). Upon cooling from the melt at 170 °C, the samples crystallize and exhibit two exotherms, occurring around 130 °C and in the range of 60–90 °C. The sharp higher temperature exotherm reflects crystallization into the paraelectric phase; the broader, more complex lower exotherm reflects the phase transition (Curie transition) to the ferroelectric crystalline phase.

Fig. 2(b) and (c), respectively, show the thermal behavior of the Nanomer and Lucentite nanocomposites as a function of composition. We observe almost no change of the mean temperature of the higher temperature melt-to-paraelectric crystallization exotherm at 2% OMS content. Only for 10, 18 and 25% OMS was there a depression of the melt-to-paraelectric transition. However, elevation of the lower temperature exotherm (paraelectric-to-ferroelectric phase transition) was observed for all OMS compositions. The exo- and endothermal peak positions and heats of crystallization are summarized in Table 2. Note that the heat of crystallization reported in Table 2 has been normalized to co-polymer content in the composites, but the curves in Fig. 2 have not been corrected.

In Fig. 2(a), the co-polymer (solid line) possesses a resolved double exotherm at the paraelectric-to-ferroelectric phase transition. It has been suggested that this arises from the existence of two paraelectric and two ferroelectric

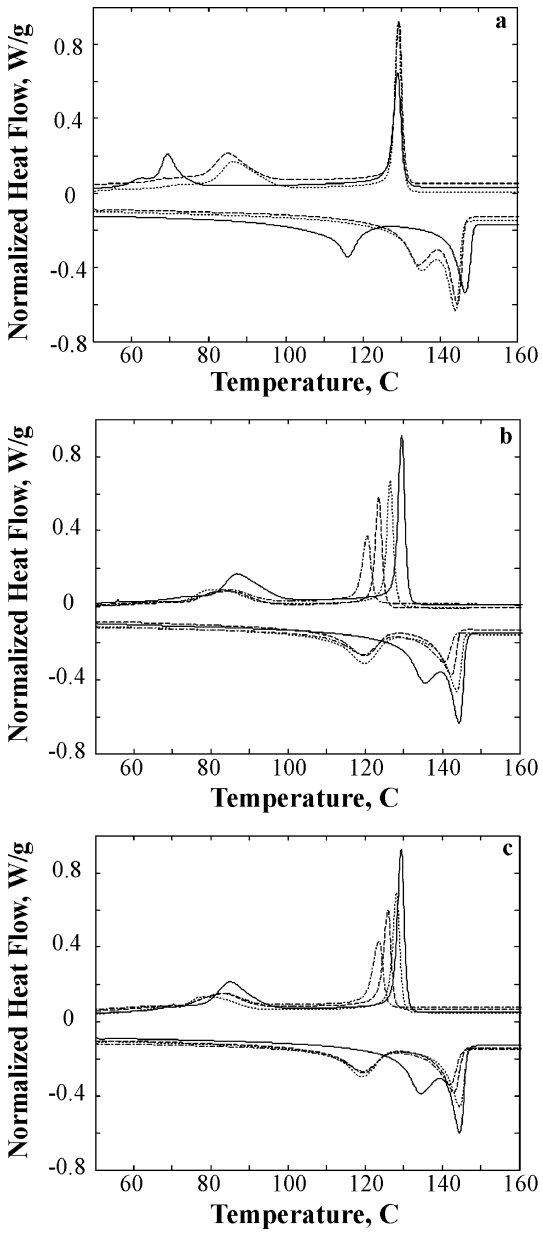

Fig. 2. DSC heat flow vs. temperature during first cooling and second heating. (a) 75/25 P(VDF-TrFE) co-polymer (solid line); 75/25 P(VDF-TrFE) + 2% Lucentite OMS nanocomposite (dotted line); 75/25 P(VDF-TrFE) + 2% Nanomer OMS nanocomposite (dashed line). (b) 75/25 P(VDF-TrFE) + Lucentite OMS nanocomposites; (c) 75/25 P(VDF-TrFE) + Nanomer OMS nanocomposites. For (b) and (c), OMS content by weight is indicated as follows: 2%—solid line, 10%—dotted line, 18%—dashed line, or 25%—dash-dot line.

phases [22,23]. Addition of either OMS results in a single broad exotherm associated with the Curie transition. The effect on the transition temperatures depends upon OMS composition. At 2% OMS, no change in melt-to-paraelectric transition temperature is observed. Higher OMS compositions depress the melt-to-para exotherm to lower temperatures, while increasing the temperature of the para-to-ferroelectric phase transition. Upon reheating, the separation between the ferroelectric-to-paraelectric and paraelectric-to-melt

Table 2
Thermal transition heats and peak temperatures for P(VDF-TrFE)/OMS nanocomposites

Sample	OMS (%)	ΔH_{c1} (J/g)[a]	T_{c1} (°C)[a]	T_{c2} (°C)[b]	T_{m1} (°C)[c]	T_{m2} (°C)[d]
75/25[e]	0	31.4	129.2	69.2	116.2	146.6
N	2	36.6	129.3	85	134.7	144.5
N	10	31.7	128.2	80.2	119.3	144.6
N	18	30.8	126	83.4	120	141.7
N	25	28.4	123.5	82.9	119.7	142
L	2	35.9	129.2	86.7	135.1	144
L	10	30.7	126.5	81	120	143.8
L	18	29.1	123.5	84	119.8	142.3
L	25	24.6	120.3	84.4	119.7	140.5

[a] Melt to para.
[b] Para to ferro.
[c] Ferro to para.
[d] Para to melt.
[e] 75/25 refers to copolymer; N refers to Nanomer OMS; L refers to Lucentite OMS.

transitions is considerably narrower in the composites than in the co-polymer control. Since some ferroelectric crystals are converted to paraelectric ones *at the same time* as some paraelectric crystals are melting (crystallization of the paraelectric phase extends to quite a low temperature), it is difficult unambiguously to resolve individual heats of transition either during heating, or for the Curie transition on cooling.

The addition of 2% OMS results in a significant increase in heat of crystallization compared to the neat co-polymer (see Table 2). This is accompanied by an estimated ~50% increase in area of the lower temperature exothermic peak associated with formation of ferroelectric crystals. The normalized crystallinity developed for the 10% composite is comparable to the neat co-polymer, while the other compositions exhibit crystallinities below the unmodified copolymer. Dispersed layered silicates (modified and unmodified) have been demonstrated to act as nucleating agents, and hence speed up the crystallization process, of some semi-crystalline polymers [24,25]. In other cases, like the situation here, the OMS has been found to nucleate crystallization at lower OMS contents, but act to retard crystallization at higher concentrations [26,27]. The latter behavior has been proposed to arise from reduced diffusion of chain segments to the sites of crystallization [25].

Determination of degrees of crystallinity from heats of crystallization is limited by uncertainty in the equilibrium heat of fusion/crystallization (ΔH_f^0) for the75/25 P(VDF-TrFE) copolymer. Extrapolation of the heats of fusion in Ref. [28] for a 78/22 VDF/TrFE copolymer yields an approximate ΔH_f^0 of ca. 38 J/g. However, a detailed review of reported heats of fusion for similar copolymers (and terpolymers), particularly from the work of Zhang et al. [29], suggests that ΔH_f^0 for VDF-TrFE copolymers with compositions near 75/25 are in the range of 40–45 J/g. Using the latter value to estimate the crystallinities leads to about 70% crystallinity for the neat 75/25 copolymer, ~80% P(VDF-TrFE) crystallinity for the 2% OMS composites, and down to as low as ~55% crystallinity of the co-polymer in the 25% Lucentite composite. These degrees of crystallinity are dependent upon the thermal treatment history, which in the present study is non-isothermal cooling at a fixed rate. The effects of other thermal treatments on the ultimate degree of crystallinity are not reported here but will be presented in a future publication. In particular, our next report will detail the impact of high temperature isothermal treatment during formation of the paraelectric phase, on the subsequent crystallization of the ferroelectric phase in P(VDF-TrFE)/OMS nanocomposites.

3.2. FTIR studies

Fig. 3(a) and (b) shows the FTIR spectra from 600 to 1600 cm^{-1} of films examined in ATR mode. All nanocomposites exhibit a characteristic absorption band near 1281 cm^{-1}, which arises from long trans sequences of the beta phase, similar to the PVDF homopolymer [30]. We observed no bands characteristic of the non-polar alpha form of PVDF, or indeed of any other crystalline phase except those analogous to the beta-phase of PVDF. In the upper portion of the figure, the locations of major absorption bands (in cm^{-1}) are listed. For the copolymer (Fig. 3(a)) these are all quite similar to those measured for beta phase of PVDF [31]. As seen in Fig. 3(b), there is no systematic variation of the frequencies upon addition of OMS to the co-polymer.

In addition to the bands from the co-polymer, the nanocomposites exhibit two principal absorptions in this frequency range, at 1072 and 994 cm^{-1}, attributed to the Si–O stretching vibrations, reported for Montmorillonite clay [32]. These are the major features of the spectra of the OMS (which are not shown for the sake of brevity). In the OMS spectra these bands are unresolved but in the nanocomposites, as OMS composition increases, these bands increase in intensity and become clearly separated. The band at 1072 cm^{-1} overlaps the relatively weak band in the co-polymer appearing at 1074 cm^{-1}.

3.3. Room temperature WAXS studies

Room temperature WAXS patterns were acquired for the thermally treated P(VDF-TrFE) copolymer and the OMS nanocomposites. For comparison, the diffraction patterns of the as-received OMS powders were also determined. Fig. 4(a) shows the WAXS diffraction patterns from $2\theta = 2 - 22°$ ($\lambda = 0.154$ nm) for the neat co-polymer film, crystallized by cooling from 170 °C at 5 °C min^{-1}. The co-polymer exhibits no diffraction peaks in the low angle range of the OMS gallery spacing. A broad amorphous halo occurs with a maximum at $2\theta \sim 17–18°$, and the (110)/(200) reflection of the ferroelectric (β phase) crystals occurs at 20.2°. Additional diffraction patterns were acquired out to

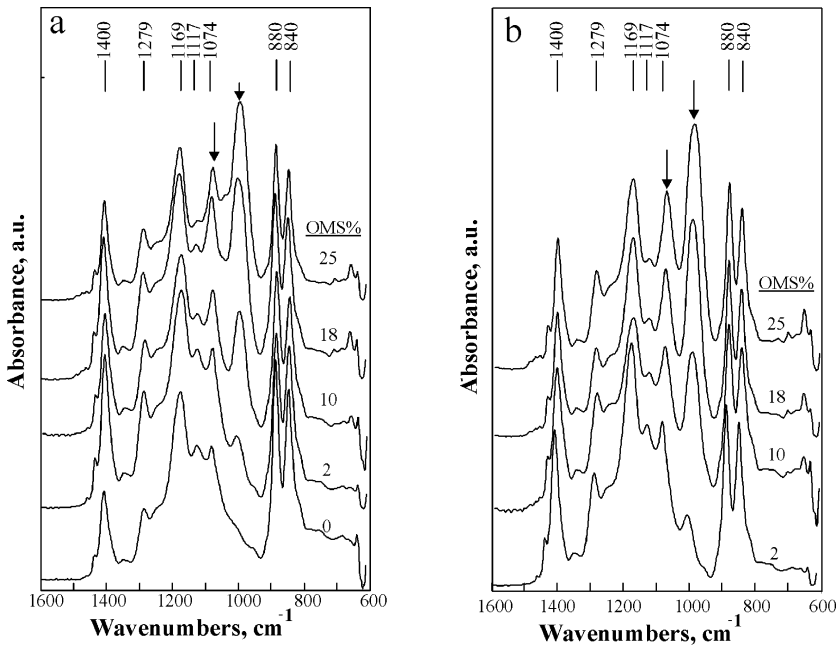

Fig. 3. FTIR absorption spectra for the indicated OMS compositions by weight: (a) 75/25 P(VDF-TrFE) copolymer (bottom curve) and 75/25 P(VDF-TrFE) + Nanomer OMS nanocomposites; (b) 75/25 P(VDF-TrFE) + Lucentite OMS nanocomposites. Arrows mark the location of two absorption bands that scale with the OMS content. At the top, the locations of the major bands of the 75/25 P(VDF-TrFE) co-polymer are shown for comparison.

higher angles, but are not shown here for the sake of brevity. No other diffraction maxima were observed up to $2\theta = 30°$.

For comparison, the inset in Fig. 4(a) shows diffraction from the galleries in the as-received Lucentite and Nanomer OMS powders. The peak assigned to the gallery spacing in the Nanomer OMS occurs as a poorly resolved doublet. The Lucentite OMS (001) gallery spacing is 1.9 nm, intermediate between the Nanomer OMS (001) doublet (*d*-spacings of 2.3 and 1.8 nm). All OMS powders exhibited a weak higher angle reflection, occurring at the location of the copolymer's ferroelectric peak. (This peak is not seen in the expanded view shown in Fig. 4(a), but can be seen in the real-time X-ray scans shown later on in Figs. 5 and 6.) *D*-spacings are listed in Table 3.

Fig. 4(b) and (c) compares the WAXS diffraction patterns as a function of OMS content for Lucentite and Nanomer composites, respectively. Here, all samples have been cooled at 5 °C min^{-1} from the melt. Both of the 2% nanocomposites (Fig. 4(b) and (c), curve 1) exhibit a strong reflection due to the copolymer ferroelectric crystal phase near $2\theta = 20°$, and a weak diffraction peak from the OMS (001). The gallery spacing is shifted to lower angles (higher *d*-spacings) in all nanocomposites, compared to the neat OMS powders. The Lucentite gallery spacing increases from 1.90 nm for neat powder (curve 1), to 2.06–2.31 nm in the Lucentite composites. The Nanomer gallery spacing peak is a weakly resolved doublet that sharpens clearly in the nanocomposite.

Both peaks in the doublet shift to higher *d*-spacing: from 2.3 and 1.8 nm in the neat Nanomer OMS powder, to 2.75 and 2.44 nm, respectively, in the crystallized 25% Nanomer OMS nanocomposite (Fig. 4(c), curve 4). The increase of the gallery spacing suggests that there is some degree of co-polymer intercalation within the OMS galleries (see Table 3). However, the change in the gallery spacing is on the order of 0.4 nm for Nanomer 25% and 0.2–0.4 nm for Lucentite 25%, somewhat smaller than the change previously observed for melt processed PVDF—OMS composites [29].

Addition of the OMS has a pronounced effect on the width of the ferroelectric X-ray reflection. As OMS composition increases to 10–25% (curves 2–4), the ferroelectric peak becomes broader and less intense compared to that of the 2% material. At the same time, the reflection

Table 3
WAXS *d*-spacings for P(VDF-TrFE)/OMS nanocomposites at 25 °C

Sample[a]	OMS (%)	d_{001} (nm)	d_{002} (nm)	*d* (nm)[b]
75/25	0	None	None	0.44
N	2	None	None	0.44
N	10	2.70, 2.07	1.35, none	0.45
N	18	2.75, 2.07	1.37, none	0.46
N	25	2.75, 2.44	1.35, 1.21	0.45
N	100[c]	2.31, 1.79	None, none	0.44[d]
L	2	2.16	1.15	0.44
L	10	2.02	1.12	0.46
L	18	2.08	1.15	0.46
L	25	2.31	1.18	0.46
L	100[c]	1.90	0.92	0.45[d]

[a] [a]Samples crystallized by cooling from 170 °C at 5 °C min^{-1}; 75/25 refers to copolymer; N refers to Nanomer OMS; L refers to Lucentite OMS.
[b] Refers to the 75/25 P(VDF-TrFE) ferroelectric crystal phase reflection, except where noted.
[c] As-received, neat OMS powder.
[d] OMS reflection.

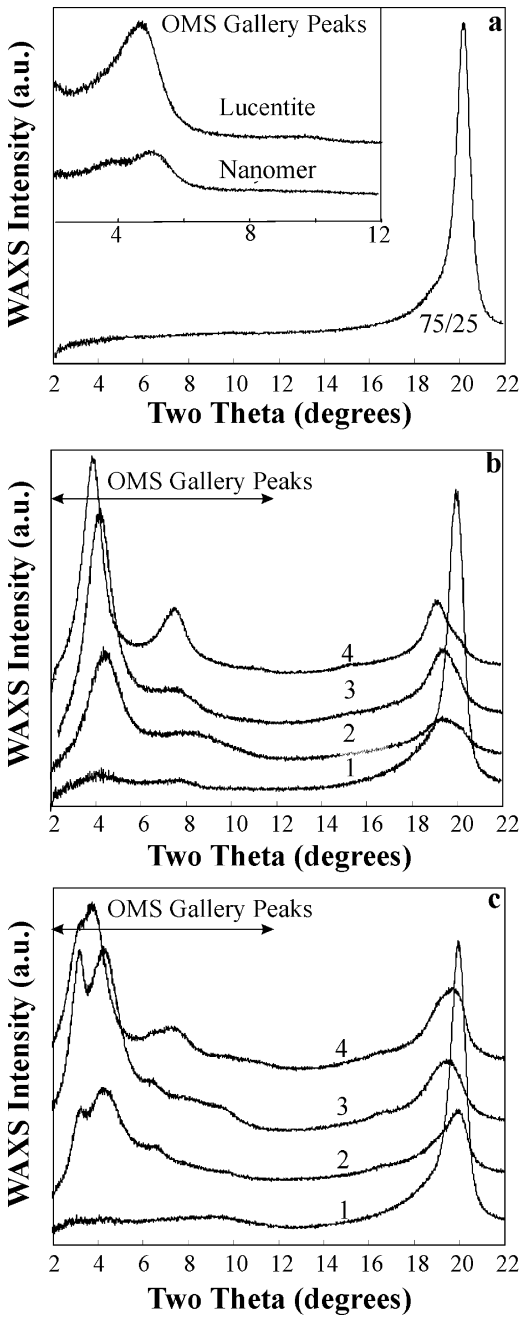

Fig. 4. WAXS intensity vs. scattering angle, 2θ (for $\lambda = 0.154$ nm). Samples were thermally treated by cooling at 5 °C min^{-1} from the melt, except for the as-received OMS powders that were examined without thermal treatment. (a) 75/25 P(VDF-TrFE) co-polymer; inset shows as-received Lucentite and Nanomer OMS powders; (b) 75/25 P(VDF-TrFE) + Lucentite OMS nanocomposites; (c) 75/25 P(VDF-TrFE) + Nanomer OMS nanocomposites. For (b) and (c), OMS contents by weight are indicated as follows: curve 1–2%, curve 2–10%, curve 3–18%, curve 4–25%. The range of the OMS gallery spacing peaks is shown with horizontal arrows.

from the gallery spacing becomes sharper and stronger as OMS composition increases. In several nanocomposite patterns, the gallery spacing is accompanied by a higher order (002) reflection.

To estimate the crystallite size, the WAXS peaks were first fitted with Gaussian profiles for evaluation of the peak breadth. The Lorentz-corrected scattered intensity, $I(q)q^2$, was fitted with a sum of Gaussians and a linear baseline term using:

$$I(q)q^2 = \sum_i \{A_i \exp((q - q_{0i})^2/2\sigma_i^2)\} + B + Cq \quad (1)$$

where A_i is the amplitude, q_{0i} is the mean q-vector, σ_i is the standard deviation, and B and C are the intercept and slope, respectively, of the linear offset.

The Gaussian fits were used to determine the coherence length, t, of the crystals in the direction perpendicular to the set of lattice planes having Miller Indices, hkl. The Scherrer equation was used to find t from: [33]

$$t = K\lambda/(\beta_{hkl} \cos \theta_{hkl}) \quad (2)$$

where K is the Scherrer constant, taken as $K \sim 0.89$ [33]. β_{hkl} is the broadening due to crystallite size effects (no lattice strain is included here), and is related to the measured peak width, B, and instrumental broadening parameter, b, for Gaussian line shapes using:

$$\beta^2 = B^2 - b^2 \quad (3)$$

Results are summarized in Table 4 for t_{ferro}, the coherence lengths corresponding to the ferroelectric peak. The small silicate peak (seen in this angular range in Figs. 5 and 6) has no effect on the full width at half maximum (FWHM), even for the 25% OMS nanocomposite. Therefore, the FWHM was determined from the experimental ferroelectric peak without subtraction of the insignificant OMS reflection that overlaps with it. The coherence length of the ferroelectric peak is largest in the 75/25 co-polymer and is only slightly reduced in the 2% OMS nanocomposites. For all larger OMS compositions, there is a dramatic drop in t_{ferro}. This is an indication that the ferroelectric phase crystals become less perfect, and not as numerous, as the amount of OMS increases. The area underneath the ferroelectric peak was used to calculate a 'crystallinity index', defined as the ratio of the crystalline peak area to the total area.

These data are listed in the last column of Table 4. The general trends are similar to those seen in the heats of crystallization (see Table 2). Both the 2 and 10% OMS nanocomposites have equal or greater WAXS crystallinity index than the 75/25 co-polymer and the index decreases for higher OMSs. However, it should be noted that the crystallinity indices derived from WAXS areas are smaller than degrees of crystallinity calculated on the basis of 45 J/g heat of fusion assumed for the perfect crystal.

3.4. Real-time WAXS studies

Fig. 5(a)–(d) shows three-dimensional plots of WAXS intensity vs. 2θ vs. temperature, for data taken at NSLS (here, $\lambda = 0.1366$ nm). The data are shown for a restricted range of 2θ, from 12 to 22°. Fig. 5(a) and (b) show the

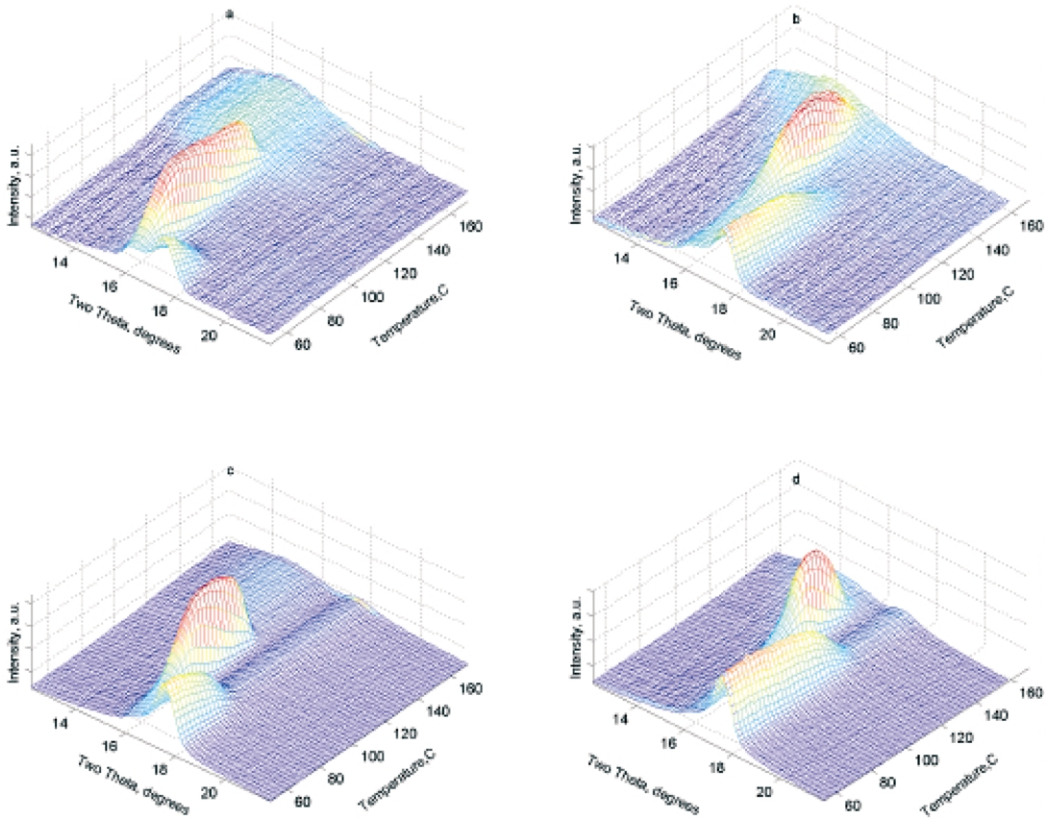

Fig. 5. WAXS intensity vs. scattering angle 2θ (for $\lambda = 0.1366$ nm) vs. temperature for: 75/25 P(VDF-TrFE) co-polymer during (a) cooling, or (b) reheating; and 75/25 P(VDF-TrFE) + 25% Nanomer OMS nanocomposite during (c) cooling, or (d) reheating.

cooling and reheating scans, respectively, for the neat 75/25 co-polymer film. Fig. 5(c) and (d) show the corresponding scans for the nanocomposite with 25% Nanomer OMS.

The cooling curve for the neat co-polymer (Fig. 5(a)) exhibits only its amorphous halo in the melt state in this angular range. When the temperature decreases to 128 °C, there is a sharp increase in scattered intensity at $2\theta = 16.3°$, (d-spacing = 0.481 nm) due to crystallization into the paraelectric phase. The intensity of this peak does not change much with further reduction in temperature, until the transition from paraelectric to ferroelectric crystal structure occurs. In the co-polymer, this transition begins at 74 °C and is signaled by the decrease in the intensity of the paraelectric peak at 16.3°, and concomitant increase in the ferroelectric peak at $2\theta = 17.4°$ (d-spacing = 0.450 nm). This transition is not as sharp as the melt-to-para transition, occurring over a wider temperature range.

Table 4
Coherence length and crystallinity index for ferroelectric peaks

Sample[a]	OMS (%)	t_{ferro} (nm)[b]	Cryst. index[c]
75/25	0	22	0.64
N	2	20	0.64
N	10	9	0.70
N	18	7	0.61
N	25	8	0.39
N	100	None	0
L	2	20	0.69
L	10	6	0.71
L	18	8	0.63
L	25	11	0.55
L	100	None	0

[a] 75/25 refers to copolymer; N refers to Nanomer OMS; L refers to Lucentite OMS.
[b] Coherence length was determined from the measured width of the reflection at half-maximum.
[c] Determined from the ratio of integrated area of the fitted Gaussian curves, to the total area, for the ferroelectric peak.

In this non-isothermal cooling treatment scheme, the lowest temperature reached is 50 °C. For the co-polymer, the paraelectric crystals are not completely converted to the ferroelectric phase at this temperature, as can be seen by the remnant of the paraelectric phase peak at 50 °C. Upon reheating from 50 °C (Fig. 5(b)) the ferroelectric phase exhibits hysteresis and persists to a temperature much higher than the paraelectric-to-ferroelectric transition temperature seen on cooling. At 114 °C the ferroelectric crystals begin to convert to the paraelectric phase, and intensity diminishes in one while growing in the other. At 149 °C, the melting of the paraelectric crystals is complete.

The cooling curve for the nanocomposite with 25% Nanomer OMS is shown in Fig. 5(c). There is a broad but weak reflection due to the OMS (at d-spacing = 0.447 nm) that can be seen in the scans of either the melt or the paraelectric phases. As temperature is decreased, we see that

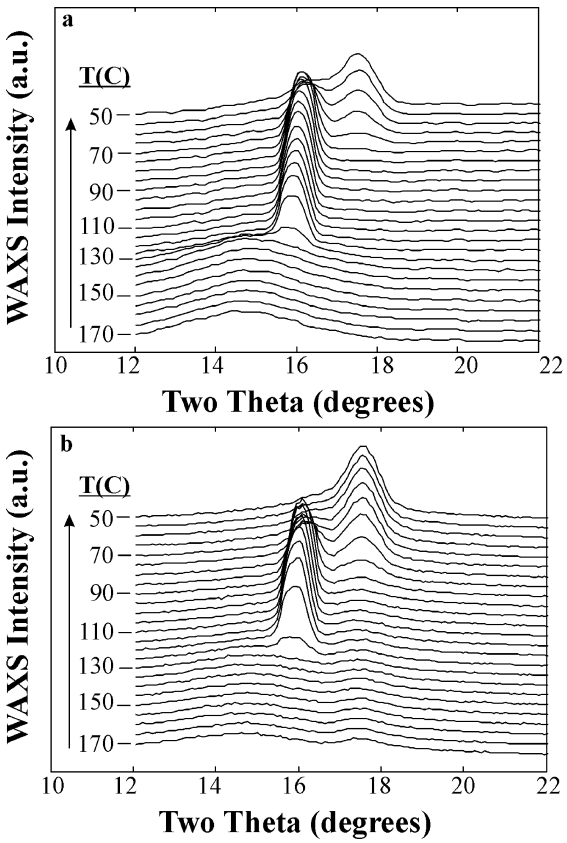

Fig. 6. WAXS intensity vs. scattering angle 2θ (for $\lambda = 0.1366$ nm) during cooling from 170 to 50 °C, for: (a) 75/25 P(VDF-TrFE) co-polymer, and (b) 75/25 P(VDF-TrFE) + 25% Nanomer OMS nanocomposite.

the melt-to-paraelectric phase transition occurs at a lower temperature of 122 °C, and the paraelectric-to-ferroelectric transition occurs at higher temperature of 89 °C. This is a 33 °C window, compared to 54 °C for the neat co-polymer. The ferroelectric crystal peak intensity remains undiminished on reheating (Fig. 5(b)) to at least 128 °C, and some ferroelectric crystals still exist at 140 °C. The paraelectric crystals begin to develop from the ferroelectric phase at 128 °C and completely melt by 148 °C.

Results for other compositions of Nanomer Lucentite OMS are not shown for brevity but may be summarized as follows. There is no change in the paraelectric or ferroelectric peak positions (no change in d-spacing) for any of the nanocomposites, compared to the neat co-polymer. Therefore, the crystals formed in the composites are the same in their inter-atomic spacing as those of the co-polymer. The increase in composition of OMS (10–25%) systematically reduces the melt-to-paraelectric transition temperature, while increasing the paraelectric-to-ferroelectric transition temperature, confirming the DSC observations presented in Fig. 2.

Fig. 6(a) and (b) shows a stacked view of WAXS intensity vs. diffraction angle (2θ) of the 75/25 P(VDF-TrFE) copolymer and P(VDF-TrFE) + 25% Nanomer OMS nanocomposite, respectively, as temperature is decreased from 170 to 50 °C. For clarity, every other data scan is removed in this presentation, and the temperature interval data are coarser than in Fig. 5. The P(VDF-TrFE) amorphous halo in the melt state is apparent at $2\theta \sim 14.5°$. At higher temperature in Fig. 6(b), a small peak arising from the OMS at $2\theta \sim 17.5°$ is observed along side the amorphous halo. As temperature decreases, growth of the paraelectric phase is indicated by the reflection at $2\theta \sim 16°$. Further decrease in temperature leads to conversion of the paraelectric crystals to ferroelectric crystals, as indicated by the growth of the reflection at $2\theta \sim 17.5°$ (smaller d-spacing).

The change in WAXS peak height was monitored as a function of temperature. In Fig. 7(a) and (b) the time development of the WAXS peak intensity for the paraelectric phase (stars) and ferroelectric phase (circles) is shown for 75/25 P(VDF-TrFE) copolymer (Fig. 7(a)) and the 75/25 P(VDF-TrFE) + 25% Lucentite OMS nanocomposite (Fig. 7(b)). Results of Gaussian fitting indicate that the width of the paraelectric crystal peak decreases slightly upon cooling. Once the ferroelectric phase crystals start to form, the paraelectric crystal peak breadth slightly increases while the ferroelectric crystal peak breadth remains nearly constant. Thus, the peak height can be used as an indictor of the crystallization kinetics, as is shown in Fig. 7. Here, the WAXS peak height is plotted during cooling and reheating.

In the temperature range where the ferroelectric phase crystal peak height is a maximum, the paraelectric phase peak height does not decrease to zero intensity. The paraelectric phase is not completely converted to ferroelectric crystals at 50 °C, so that a small paraelectric peak remains. The amount of residual paraelectric phase crystals at 50 °C is smaller in all the nanocomposites than in the 75/25 P(VDF-TrFE) co-polymer because of the increased temperature of formation of the ferroelectric phase in the nanocomposites.

Fig. 7 shows the increased stability window for ferroelectric phase crystals in the nanocomposite compared to the 75/25 co-polymer. In the copolymer, the ferro-electric phase crystals begin forming non-isothermally at 74 °C, and melt completely by 114 °C. In the 25% Lucentite OMS nanocomposite, ferroelectric crystals begin forming at higher temperature, 91.6 °C, and melt completely by 122 °C. WAXS results confirm the DSC analyses, and provide clear evidence that ferroelectric crystals form at the expense of the paraelectric crystals. Furthermore, the addition of either the Lucentite or Nanomer OMS results in an increased temperature window of stability for the ferroelectric phase crystals.

4. Conclusions

Solution processing was used to form tough nanocomposite films of P(VDF-TrFE) 75/25 co-polymer with layered silicates. Addition of Lucentite or Nanomer OMS increases the thermal stability of the films. Concentration dependent

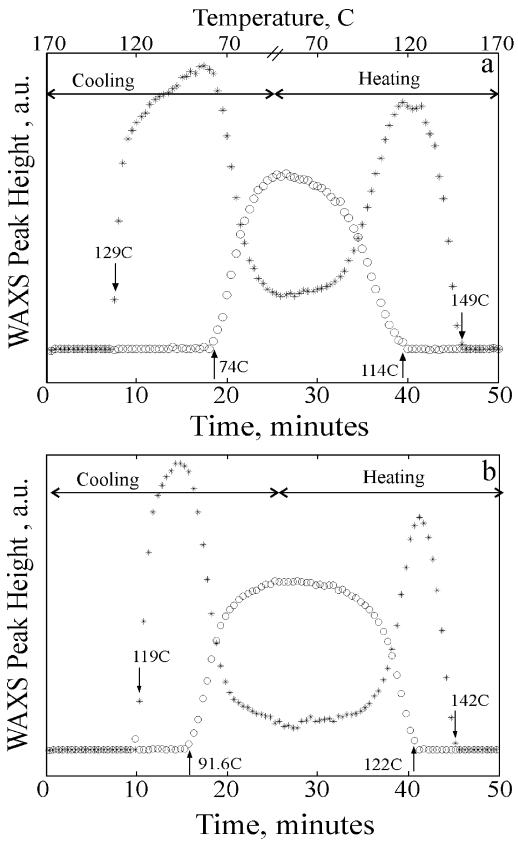

Fig. 7. WAXS peak height development with time during non-isothermal cooling and reheating at rate of 5 °C min^{-1}, from 170 to 50 to 170 °C. There is a two-minute isothermal holding period at 50 °C between cooling and reheating stages. For convenience, the temperatures are displayed on the horizontal axis above. Paraelectric phase peak (stars); ferroelectric phase peak (circles). (a) 75/25 P(VDF-TrFE) copolymer; (b) 75/25 P(VDF-TrFE) + 25% Lucentite OMS nanocomposite.

effects were observed on the thermal and structural properties. At low concentrations (2% OMS by weight), Lucentite or Nanomer OMS serve as nucleating agent for co-polymer crystallization, affecting both the melt to paraelectric phase transition and the para-to-ferroelectric transition. Transition temperatures increased during cooling, and amount of paraelectric crystals formed increased. Higher concentrations of OMS (10–25%) delayed the formation and reduced the amount of paraelectric crystals, while inducing the ferroelectric crystals to form at higher temperatures. The temperature stability range of the ferroelectric crystals was thus significantly increased in the nanocomposites.

Acknowledgements

The authors express their appreciation to the National Science Foundation, Polymers Program (DMR—0100646 and DMR—0211056) for partial support of this research. We thank Tufts undergraduate students, Ms Heather Held and Ms Megan Peal for assistance with thermal analysis, and Ms Laurel Powers for assistance with X-ray diffraction. We would also like to thank Mr Rob J. Klein for helpful discussions.

References

[1] Nakamura K, Wada Y. J Polym Sci 1971;A-2(9):161.
[2] Broadhurst MG. Ferroelectrics 1973;5:39.
[3] Lovinger A, Furukawa T, Davis D, Broadhurst M. Ferroelectrics 1983;50:227.
[4] Nalwa HS, editor. Ferroelectric polymers. New York: Marcel Dekker; 1995.
[5] Doll W, Lando J. J Macromol Sci 1970;B4:889.
[6] Lu C, Liepins R. Electrical properties of polymers: chemical principles. Munich: Hanser Publishers; 1987. p. 33.
[7] Davies GR. Physics of dielectric solids. In: Goodman C, editor. Inst. Phys. Conf. Series No. 58; 1980. p. 50.
[8] Wang TT, Herbert JM, Glass AM, editors. The applications of ferroelectric polymers. New York: Chapman & Hall; 1988.
[9] Zhang QM, Bharti V, Zhao X. Science 1998;280:2101.
[10] Casalini R, Roland CM. Appl Phys Lett 2001;79:2627.
[11] Xia F, Cheng ZY, Xu H, Zhang QM, Kavarnos G, Ting R, Abdul-Sedat G, Belfield KD. Adv Mater 2002;14:1574.
[12] Chung TC, Petchsuk A. Macromolecules 2002;35:7678.
[13] Baltá Calleja FA, González Arche A, Ezquerra TA, Santa Cruz C, Batallán F, Frick B, López Carbarcos E. Adv Polym Sci 1993;108:1.
[14] Furukawa T. Phase Transitions 1989;18:14.
[15] López Cabarcos E, de las Rivas B, Ezquerra TA, Baltá Calleja FJ. Macromolecules 1998;31:6157.
[16] Alexander M, Dubois P. Mater Sci Engng 2000;R28:1.
[17] Gianenelis EP, Krishnamoorti R, Manias E. Adv Polym Sci 1998;138:107.
[18] LeBaron PC, Wang Z, Pinnavaia TJ. J Appl Clay Sci 1999;15:11.
[19] Xu R, Manias E, Snyder AJ, Runt J. Macromolecules 2001;34:337.
[20] Xu R, Manias E, Snyder AJ, Runt J. J Biomed Mater Res 2003;64A:114.
[21] For example: Nanocor, Inc. Material safety data sheet on Nanomer I.30TC, July, 1998; Zen-Noh Unico America, Synthetic smectite data sheet available at: http://www.unicoop.co.jp/en/products/main31.asp.
[22] Gregrio R, Botta MM. J Polym Sci, Polym Phys 1998;36:403.
[23] Casalini R, Roland CM. J Polym Sci, Polym Phys 2002;40:1975.
[24] Maiti P, Nam PH, Okamoto M, Hsegawa N, Usuki A. Macromolecules 2002;35:2042.
[25] Ogata N, Kawakage S, Ogihara T. Polymer 1997;38:5115.
[26] Jimenez G, Ogata N, Kawai H, Ogihara T. J Appl Polym Sci 1997;64:2211.
[27] Fornes TD, Paul DR. Polymer 2003;44:3945.
[28] Kodama H, Takahashi Y, Furukawa T. Ferroelectrics 1997;203:433.
[29] For example: (a) Xia F, Wang YK, Li H, Huang C, Ma Y, Zhang QM, Cheng ZY, Bateman FB. J Polym Sci, Polym Phys 2003;41:797. Cheng ZY, Olson D, Xu H, Xia F, Hundal JS, Zhang QM, Bateman FB, Kavarnos GJ, Ramotowski T. Macromolecules 2002;35:664. Cheng ZY, Zhang QM, Bateman FB. J Appl Phys 2002;92:6749.
[30] Priya L, Jog JP. J Polym Sci, Polym Phys 2003;41:31.
[31] Kobayashi M, Tashiro K, Tadakoro H. Macromolecules 1975;8:158.
[32] Lochhead RY, Boykin CM. In: Krishnamoorti R, Vaia RA, editors. Polymer nanocomposites: synthesis, characterization, and modeling. ACS Symposium Series 804, Washington, DC: American Chemical Society; 2002. p. 85–98.
[33] Warren BE. X-ray diffraction. New York: Dover Publications; 1990.